Fabrication of high-quality epitaxial $Bi_{1-x}Sb_x$ films by two-step growth using molecular beam epitaxy

K. Ueda, Y. Hadate, K. Suzuki, and H. Asano

Dept. of Materials Physics, Graduate School of Engineering, Nagoya University,

Furo-cho, Chikusa-ku, Nagoya 464-8603, Japan

Abstract

High-quality epitaxial $Bi_{1-x}Sb_x$ (BiSb) films were formed by two-step growth using molecular beam epitaxy. The use of two-step growth, which involves lower-temperature growth at ~150 °C followed by higher-temperature (~250 °C) growth, and lattice-matched substrates such as BaF_2 (111) are key to obtain high-quality BiSb films. The composition of the BiSb films can also be systematically tuned using this growth procedure. The epitaxial BiSb films showed higher crystallinity (full width at half maximum: ~0.69°) and higher mobility (~2100 cm^2/Vs), which indicate that sufficient quality films were obtained. Such films are expected to pave the way for the fabrication of electronic devices using topological BiSb.

Keywords: Bismuth antimonide; Thin films; Two-step growth; Molecular beam epitaxy; Topological materials; Mobility

1. Introduction

Topological materials such as topological insulators and topological semimetals have attracted much attention because of their interesting physical properties due to their topologically protected surface states with linear band dispersion [1, 2]. These materials are interesting not only from physical viewpoints but also with respect to electronic applications, because of their extremely high mobility and spin polarization (helical spin polarization). Many chalcogenide compounds such as Bi_2Te_3, Bi_2Se_3, and PbTe have recently been found to have topological characteristics and are considered to be promising materials for electronic applications [1, 2]. Film fabrication of topological materials is one of most important steps for electronic applications. Thin films of several topological chalcogenide compounds such as Bi_2Te_3 and Bi_2Se_3 have been fabricated using various methods, such as molecular beam epitaxy (MBE) [3-5] and chemical vapor deposition (CVD) [6]. However, it is not easy to obtain high-quality topological chalcogenide films and there is room for improvement. We consider the degradation of film quality in these chalcogenide films is mainly due to the high volatility of chalcogenides such as Se and Te, which leads to lower tunability of the composition, the formation of a large number of defects, and the need to use lower growth temperatures (<200 °C). The strong toxicity of chalcogenides is also problematic for applications.

We focused on topological $Bi_{1-x}Sb_x$ (BiSb) because of the non-inclusion of toxic and highly volatile elements such as Se and Te. The topological characteristics of BiSb appear when the Sb composition is above 4% [7-10], and the material becomes a topological semimetal for x= 0.04–0.07 and a topological insulator for x= 0.07–0.22. The lower toxicity BiSb compounds also exhibit interesting physical properties such as

large spin Hall effects [11] and extremely large magnetoresistance [12, 13]. However, there are fewer studies on BiSb than on topological chalcogenides such as Bi_2Se_3 and Bi_2Te_3 because BiSb is considered to be unsuitable for physical research on topological surface states due to the complicated surface band structure [7, 14]. On the other hand, we consider that BiSb is important with respect to electronic applications because the fabrication of high-mobility (~10^4 cm^2/Vs) samples with lower defect densities is easier than for other topological materials [13, 15]. The non-inclusion of highly toxic and volatile elements such as Se, Te, and As is another advantage of BiSb. However, there is only a modest number of reports on the growth of BiSb films [16-18], and only limited information on the growth and crystalline quality of BiSb films. Also, there is room for improvement of BiSb film quality.

In this study, high-quality epitaxial BiSb thin films were fabricated using MBE and their structural and electronic characteristics were examined in detail toward the fabrication of electronic devices using topological BiSb. As described later in detail, two-step growth [3, 19-21] was necessary for the growth of high-quality BiSb films.

2. Experimental methods

$Bi_{1-x}Sb_x$ (x= 0–0.44) films were grown on BaF_2 (111) and GaAs (111) substrates by K-cell MBE with pure Bi and Sb sources at a growth temperature (T_g) of 100–300 °C. The growth rate was 3–7 nm/min and the typical film thickness was ~300 nm. The growth rate was determined by thickness measurements using step gauge (Dektak surface profiler). The BaF_2 substrates were annealed in a vacuum at 500 °C prior to the growth process to clean the substrate surface [22]. BaF_2 (111) substrates are often used for the growth of pure Bi films [23]; however, there are few reports on the growth of

BiSb films on BaF_2 (111). The T_g was set just below the solid-liquid phase boundary for the Bi-Sb system [24] to obtain higher-quality BiSb films. The lattice mismatch between BiSb (x= 0.1) and the BaF_2 (111) and GaAs (111) substrates is 3.2% and 13.1%, respectively. This mismatch changes depending on the Sb composition in BiSb. Structural characterization of the BiSb films was performed using X-ray diffraction (XRD) with a Cu K_α radiation source (λ= 1.54Å) [out-of-plane (2θ-θ) XRD measurements from 20° to 100° and rocking curve measurements using Rigaku Ultima IV and other XRD measurements such as ϕ-scan from 0° to 360° and reciprocal space mapping using Rigaku SmartLab]. The compositions of the BiSb films were determined using energy dispersive X-ray spectroscopy (EDX-SEM) (Hitachi S5200). The accelerating voltage and spectrum range were set to 30 kV and 12000 eV for the EDX analysis, respectively. The electronic properties of the BiSb films were investigated by Hall measurements (van der Pauw method) from ~20 K to room temperature (RT) under a magnetic field of 0.5 T.

3. Results and discussion

Bi has a lower sticking coefficient due to its lower melting point (271 °C) and relatively high volatility, which makes the fabrication of BiSb films difficult. T_g was restricted to below 280 °C because of the lack of adhesion of BiSb films (x= 0.03–0.44) above 300 °C. Therefore, film growth of BiSb was performed using two-step growth; T_g was lower at the initial stage to increase the adhesion rate of BiSb and was then higher at the second stage to improve crystallinity. The two-step growth procedure is often used for the film growth of topological chalcogenides [3, 19, 20]. For comparison, BiSb films were also fabricated by a conventional procedure, where T_g was fixed at one

specific temperature (250 °C in this case).

Figure 1(a) shows out-of-plane (2θ-θ) XRD patterns for BiSb films (x= ~0.1) formed on BaF_2 (111) substrates by the conventional procedure (one-step growth) and two-step growth. For one-step growth, many peaks from various planes of BiSb were observed in the XRD pattern; these BiSb films were also nonuniform and insulating. These results suggest that nonuniform polycrystalline BiSb films were formed by one-step growth and these films were unsuitable for use in electronic applications. On the other hand, in the case of two-step growth (T_g = 150 °C → 250 °C), only the (00l) peaks for the BiSb films, apart for the substrate peaks, were observed in the XRD pattern, which indicates c-axis orientation of the films [Fig. 1(a), lower pattern]. The c-axis lattice constant for the BiSb films was estimated to be 1.183 nm, which was comparable to that for bulk $Bi_{0.9}Sb_{0.1}$ (1.181 nm) [25]. The full width at half maximum (FWHM) of the (003) peak in the BiSb film pattern was estimated to be 0.69°, which suggests that the BiSb film has good crystallinity. These results indicate that highly crystalline c-axis oriented BiSb films can be formed on BaF_2 substrates by two-step growth. C-axis oriented Bi (x= 0) films were obtained by one-step growth on BaF_2 (111) substrates, although a lower T_g of ~100 °C was required. The crystalline quality of the Bi films was improved using two-step growth (T_g= 100 °C → 250 °C) and the Bi (003) XRD peak intensity became one order of magnitude higher than that obtained with one-step growth.

Figure 1(b) shows the (003) XRD peak intensity as a function of the growth temperature at the initial stage (T_{ini}). T_{ini} was changed to determine the optimum growth conditions for two-step growth. T_g in the second stage was fixed at 250 °C. BiSb films formed at T_{ini} = 150-170 °C became single crystal (c-axis oriented films) and the peak intensity at T_{ini} = 150 °C was twice that obtained at T_{ini} = 170 °C. In contrast, BiSb films

formed below T_{ini} = 130 °C or above 200 °C became polycrystalline, probably because of the lower migration energy at lower temperature or the lower adhesion rate at higher temperature. These results indicate that T_{ini} = 150 °C is the optimum temperature for the initial stage of two-step growth of BiSb films. As a note, the growth rate of the BiSb films for the condition (T_g = 150-> 250°C) was ~3-4 nm/min.

Figure 2 shows SEM images of the BiSb films on BaF_2 (111) substrates formed by 2-step growth with various T_{ini}. Grain structures were clearly observed on the surfaces of the BiSb films, and there were no precipitates like structures on the surfaces. The grain size was increased from 1 μm to several μm as T_{ini} increased, indicating higher crystallinity for higher T_{ini}. In the case for T_{ini}= 200°C, surface morphology was changed and many void like structures were observed with larger grains. This is probably originated from lower sticking coefficients of Bi for higher T_{ini}. These SEM results agree with T_{ini} the dependence of (003) intensity, which shows tendency for higher crystallinity for higher T_{ini} [Fig. 1(b)].

Figure 3(a) shows out-of-plane XRD patterns around the (003) peak for BiSb films with various Sb compositions (x= 0.04–0.44) on BaF_2 (111) substrates formed using two-step growth. T_{ini} was fixed at 150 °C and the typical thickness for the initial stage was set to ~100 nm. T_g for the second growth stage was increased from 250 °C to 280 °C as the Sb concentration increased to improve the crystalline quality of the Sb-richer films (250 °C for x ≤ ~0.2, 260 °C for x = ~0.3, 280 °C for x = ~0.4). BiSb films with a c-axis orientation and various Sb concentrations could be obtained by two-step growth. The (003) peak position systematically moved to higher angle as the Sb concentration increased, which indicated a systematic decrease the of c-axis lattice constant. As a note, broad peak at ~24.5° As shown in Figure 3(b), the c-axis lattice

constant (*c*) decreased in proportion to the Sb concentration, thereby obeying the Vegard law (*c* (nm) = 1.1862(1-x) + 1.1274x), where x is the Sb concentration, and *c* for pure Bi and Sb is taken to be 1.1862 and 1.1274, respectively [27]. This means that the composition of BiSb films can be determined from XRD measurements without using a direct compositional analysis method such as EDX. These results suggest the composition of the BiSb films could be systematically controlled and BiSb films with various compositions could be formed by two-step growth. However, the intensity of the (003) XRD peak decreased as the Sb concentration increased [Fig. 3(a)], which is considered to be related to the lower migration energy in Sb-rich BiSb films, and the crystalline quality of the Sb-rich BiSb films have much room for improvement. The quality of the Sb rich films will be improved in the near future by optimization of film growth conditions such as the initial and/or second growth temperature and the growth rate.

Figure 4(a) shows in-plane XRD measurement results (ϕ-scan) for the (012) peaks for the BiSb films (x= ~0.1) formed on BaF_2 (111) substrates. The BiSb (012) peaks have a three-fold symmetry as expected, and the ϕ values for the (012) peaks were the same as those for the (-111) peaks of the BaF_2 substrates. The in-plane and out-of-plane [Fig. 1(a)] XRD results suggest that the BiSb films were epitaxially grown on the BaF_2 substrates with epitaxial relationships of BiSb (001) [2-10] // BaF_2 (111) [1-10], which means the triangle plane formed by Bi (or Sb) atoms is on the triangle (111) plane of BaF_2 without rotation.

Figure 4(b) shows the reciprocal space mapping (RSM) for the BiSb films formed on BaF_2 (111) substrates; the image shows around BiSb (2-19) and BaF_2 (135). The crystal systems of BiSb and BaF_2 are different, so it is not easy to obtain information on the

strain in the films at a glance by using the RSM image. However, the BiSb films were considered to be relaxed on the BaF_2 substrates because the in-plane (*a*) and out-of-plane (*c*) lattice constants for BiSb were estimated to be 0.449 nm and 1.183 nm, respectively, from the RSM image and the XRD results [Figs. 1(a) and 4(a)], which are consistent with the lattice constants for bulk BiSb (*a*= 0.452 and *c*= 1.181 nm for x= 0.1 [25]). These results suggest that almost fully relaxed BiSb films were formed on the BaF_2 substrates. The reason for the film relaxation is the relatively large thickness of the BiSb films (~300 nm). The fabrication of strained BiSb films will be performed in the near future.

GaAs (111) substrates are often used for the growth of BiSb films [16, 27], although the lattice mismatch with GaAs (~13%) is much larger than that with BaF_2 substrates (~3%). To examine the effects of the lattice mismatch, BiSb films were also formed on GaAs substrates by two-step growth. Figure 5(a) shows an out-of-plane XRD pattern for BiSb film (x= ~0.1) on a GaAs (111) substrate formed using the same T_g (150 °C→ 250 °C) for the films grown on BaF_2 substrates. In the XRD pattern for the BiSb film on GaAs, only the (00*l*) peaks of BiSb except the substrate peaks, were observed, which indicates that a c-axis-oriented BiSb film was formed. The c-axis lattice constant for the BiSb film was estimated to be 1.181 nm, which was the same as that for bulk $Bi_{0.9}Sb_{0.1}$ (1.181 nm) [25]. The FWHM of the (003) peak for the BiSb film on the GaAs (111) substrate was 0.98°, which indicates good crystallinity. However, the FWHM for the film on GaAs is larger than that on BaF_2 (FWHM: 0.69°), which indicates lower crystalline quality for the film on the GaAs substrate. We consider this to be due to the larger lattice mismatch between BiSb and GaAs.

Figure 5(b) shows an in-plane ϕ-scan of the BiSb film formed on the GaAs (111)

substrate. The (012) peaks for the BiSb film on GaAs are much smaller and broader than those on BaF_2 [Fig. 4(a)], which indicates a lower in-plane orientation of the BiSb films on GaAs. The BiSb (012) peaks also have six-fold symmetry, which suggests in-plane two-domain formation [28, 29] for the BiSb films on GaAs. These XRD results suggest that the BiSb films are not epitaxially grown on GaAs substrates and have in-plane twin structures. There is also a possibility that the in-plane domain boundary deteriorates the electronic properties of the BiSb films. The mobility values for the BiSb films on GaAs have a tendency to show smaller values than those on the BaF_2 substrates. These XRD results indicate that it is important to adopt lattice matched substrates for the fabrication of high-quality epitaxial BiSb films, and that the BiSb film on a BaF_2 substrate showed higher crystalline quality than that on a GaAs substrate. Fan et al., performed two step growth of BiSb films by sputtering [21] and obtained good crystalline, c-axis oriented BiSb films on sapphire C substrates in spite of larger mismatch (~5.3%) between BiSb and sapphire C. However, their BiSb films have in-plane twin structures probably originated from larger lattice mismatch. We consider their results also support one of our conclusions that the use of lattice-matched substrates such as BaF_2 (111) is necessary to obtain high-quality and epitaxial BiSb films.

Figures 6(a) and 6(b) show resistivity vs. temperature (ρ-T) curves and Hall measurement results for the BiSb (x= 0.04, 0.10, and 0.16) films formed by two-step growth on BaF_2. $Bi_{0.96}Sb_{0.04}$ corresponds to a topological semimetal (TSM) phase, while $Bi_{0.90}Sb_{0.10}$ and $Bi_{0.84}Sb_{0.16}$ correspond to topological insulator (TI) phases in the electronic phase diagram of BiSb [8, 9]. The resistivity decreased with temperature for the $Bi_{0.96}Sb_{0.04}$ film, which is typical metallic behavior. The resistivity was very weakly

dependent on temperature, which suggests semimetallic characteristics for the $Bi_{0.96}Sb_{0.04}$ film. The electron concentration in the $Bi_{0.96}Sb_{0.04}$ film was estimated to be ~5×10^{19} cm^{-3} from Hall measurements, which was several orders smaller than those for typical metals (10^{22}-10^{23} cm^{-3}) and consistent with the semimetallic nature of $Bi_{0.96}Sb_{0.04}$ [12, 30]. On the other hand, for the $Bi_{0.90}Sb_{0.10}$ and $Bi_{0.84}Sb_{0.16}$ films, semiconducting behavior was observed from RT to ~100 K, which corresponds to gap opening of the BiSb films with higher Sb. The energy gap for the films was estimated to be ~3 meV from the temperature dependence of the carrier concentration. As a note, the magnetic field dependence of Hall voltage was almost linear with negative slope (correspond to n-type conductivity) in the magnetic field of $-0.5 \sim 0.5$ T for the BiSb films. The ρ-T curve for $Bi_{0.90}Sb_{0.10}$ and $Bi_{0.84}Sb_{0.16}$ changed to metallic behavior below ~100 K, probably because of higher mobility at lower temperature, which represents an increase in the mean free path for carriers in the BiSb films. The x(Sb) dependence of the ρ-T curves agrees with those of bulk BiSb [10], and also agree with recent results on MBE-grown BiSb thin films for thicker cases (~50-100 nm) [27, 31] though other factors such as quantum effects and contribution of the surface conductivity should be considered for thinner (< several tens nm) BiSb films. The mobility increased as the temperature decreased and reached 2100, 1589, and 1441 cm^2/Vs at ~20 K for the $Bi_{0.96}Sb_{0.04}$, $Bi_{0.90}Sb_{0.10}$, and $Bi_{0.84}Sb_{0.16}$ films, respectively. The relatively high mobilities also support the higher crystalline quality of the BiSb films. The mobility decreased as the Sb concentration increased, which was considered to be related to the lower crystallinity of the Sb-rich BiSb films [Fig. 3(a)]. The electronic properties of the BiSb films are consistent with those derived from the electronic phase diagram for BiSb [7-9], which suggests that the Sb concentration in the BiSb films was precisely

controlled. However, it is necessary to confirm the topological characteristics of the BiSb films by quantum oscillation [10, 32] and/or angle-resolved photoemission spectroscopy (ARPES) measurements [8, 9], and this will be a subject for future study. The structural and electronic measurement results confirmed that high-quality epitaxial BiSb films can be formed on lattice matched BaF_2 (111) substrates by two-step growth using MBE.

4. Conclusions

High-quality epitaxial BiSb films could be fabricated by two-step growth. The use of a lower T_{ini} of ~150 °C followed by a higher T_g of ~250 °C and lattice matched substrates such as BaF_2 (111) are keys to obtain high-quality BiSb films. The composition of the films could be systematically controlled using the two-step growth method. The epitaxial BiSb films have higher crystallinity (FWHM: 0.69°) and higher mobility (~2100 cm^2/Vs at 20 K), which represent sufficient quality for the fabrication of electronic devices. We consider that high-quality BiSb films based on this work will pave the way for the realization of electronic devices using topological BiSb.

Acknowledgements

The authors thank Prof. Hotta for assistance in setting up the MBE chamber for BiSb film growth. This work was supported in part by the Iwatani Naoji Foundation.

References

[1] B. Yang and S-C. Zhang, “ Topological materials” Rep. Prog. Phys. 75 (2012) 096501-1-23.

[2] Y. Ando, “Topological insulator materials”, J. Phys. Soc. Jpn., 82 (2013) 102001-1-32.

[3] L. He, X. Kou, Nd K. L. Wang, “Review of 3D topological insulator thin-film growth by molecular beam epitaxy and potential applications”, Phys. Stat. Solidi RRL 7 (2013) 50–63.

[4] A. A. Taskin, S. Sasaki, K. Segawa, and Y. Ando, “Manifestation of Topological Protection in Transport Properties of Epitaxial Bi_2Se_3 Thin Films”, Phys. Rev. Lett. 109 (2012) 066803.

[5] C. I. Fornari, P. H. O. Rappl, Sergio L. Morelhao, and E. Abramof, “Structural properties of Bi_2Te_3 topological insulator thin films grown by molecular beam epitaxy on (111) BaF_2 substrates”, J. Appl. Phys., 119, (2016) 165303.

[6] Z. Wang, M. L. Liang Y. Z. Zhang, and X. P. A. Gao, “Broadband photovoltaic effect of n-type topological insulator Bi_2Te_3 films on p-type Si substrates”, Nano Research, 10 (2017) 1872–1879.

[7] D. Hsieh, D. Qian, L. Wray, Y. Xia, Y. S. Hor, R. J. Cava, and M. Z. Hasan, “A topological Dirac insulator in a quantum spin Hall phase”, Nature 452 (2008) 970-975.

[8] H. M. Benia, C. Straßer, K. Kern, and C. R. Ast, “Surface band structure of $Bi_{1-x}Sb_x$ (111)”, Phys. Rev. B 91 (2015) 161406 (R)-1-5.

[9] H. Guo, K. Sugawara, A. Takayama, S. Souma, T. Sato, N. Satoh, A. Ohnishi, M. Kitaura, M. Sasaki, Q.-K. Xue, and T. Takahashi, “Evolution of surface states in $Bi_{1-x}Sb_x$ alloys across the topological phase transition”, Phys. Rev. B 83 (2011) 201104

(R)-1-4.

[10] A. A. Taskin, and Y. Ando, “Quantum oscillations in a topological insulator $Bi_{1-x}Sb_x$”, Phys. Rev. B 80, (2009) 085303-1-6.

[11] N. H. D. Khang, Y. Ueda, and P. N. Hai, “A conductive topological insulator with large spin Hall effect for ultralow power spin–orbit torque switching, Nature Mater., 17 (2018) 808-813.

[12] Z. J. Yue, X. L. Wang, and S. S. Yan, “Semimetal-semiconductor transition and giant linear magnetoresistances in three dimensional Dirac semimetal $Bi_{0.96}Sb_{0.04}$ single crystals”, Appl. Phys. Lett., 107, (2015) 112101-1-4.

[13] G. N. Kozhemyakin, and S. A. Zayakin, “Magnetoresistance in doped $Bi_{0.85}Sb_{0.15}$ single crystals”, J. Appl. Phys. 122 (2017) 205102.

[14] A. Nishide, A. A. Taskin, Y. Takeichi, T. Okuda, A. Kakizaki, T. Hirahara, K. Nakatsuji, F. Komori, Y. Ando, and I. Matsuda1, “Direct mapping of the spin-filtered surface bands of a three-dimensional quantum spin Hall insulator”, Phys. Rev. B 81 (2010) 041309 (R)-1-4.

[15] D-X. Qu, S. K. Roberts, and G. F. Chapline, “Observation of huge surface hole mobility in the topological insulator $Bi_{0.91}Sb_{0.09}$ (111)”, Phys. Rev. Lett. 111 (2013) 176801-1-5.

[16] K. Yao, N. H. D. Khang, and P. N. Hai, “Influence of crystal or orientation and surface termination on the growth of BiSb thin films on GaAs substrates”, J. Cryst. Growth, 511 (2019) 99-105.

[17] T. Hirahara, Y. Sakamoto, Y. Saisyu, H. Miyazaki, S. Kimura, T. Okuda, I. Matsuda, S. Murakami, and S. Hasegawa, “Topological metal at the surface of an ultrathin $Bi_{1-x}Sb_x$ alloy film”, Phys. Rev. B 81 (2010) 165422-1-5.

[18] C. Rochford, D. L. Medlin, K. J. Erickson, and M. P. Siegal, “Controlling compositional homogeneity and crystalline orientation in $Bi_{0.8}Sb_{0.2}$ thermoelectric thin films”, APL Materials 3 (2015) 126106-1-6.

[19] N. Bansal, Y. S. Kim, E. Edrey, M. Brahlek, Y. Horibe, K. Iida, M. Tanimura, G-H. Li, T. Feng, H-D. Lee, T. Gustafsson, E. Andrei, S. Oh, “Epitaxial growth of topological insulator Bi_2Se_3 film on Si(111) with atomically sharp interface”, Thin Solid Films 520 (2011) 224–229.

[20] H. D. Li, Z. Y. Wang, X. Kan, X. Guo, H. T. He, Z. Wang, J. N. Wang, T. L. Wong, N. Wang, and M. H. Xie1, “The van der Waals epitaxy of Bi_2Se_3 on the vicinal Si(111) surface: an approach for preparing high quality thin films of a topological insulator”, New J. Phys., 12 (2010) 103038-1-11.

[21] T. Fan, M. Tobah, T. Shirokura , N. Huynh D. Khang, and P. N. Hai, “Crystal growth and characterization of topological insulator BiSb thin films by sputtering deposition on sapphire substrates”, Jpn. J. Appl. Phys. 59 (2020) 063001-1-5.

[22] P. Dziawa, B. Taliashvili, W. Domuchowski, L. Kowalczyk, E. Łusakowska, A. Mycielski,V, Osinniy, and T. Story, “Structural and optical characterization of epitaxial layers of CdTe/PbTe grown on BaF_2 (111) substrates”, Phys. Stat. Sol. (c) 2 (2005) 1167–1171.

[23] S. Xiao, D. Wei, and X. Jin, “Bi (111) Thin Film with Insulating Interior but Metallic Surfaces”, Phys. Rev. Lett., 109 (2012) 166805-1-5.

[24] H. Okamoto, “Bi-Sb (Bismuth-Antimony)”, J. Phase Equil. Diff. 33 (2012) 493–494.

[25] P. Cukka, and C. S. Barret, “The crystal structure of Bi and of solid solutions of Pb, Sn, Sb and Te in Bi”, Acta. Cryst. 15 (1962) 865-872.

[26] D. Schiferl and C. S. Barrett, “The crystal structure of arsenic at 4.2, 78, 299 K”, Journal of Applied Crystallography 2 (1969) 30-36.

[27] Y. Ueda, N. Huynh D. Khang, K. Yao, and P. N. Hai, “Epitaxial growth and characterization of $Bi_{1-x}Sb_x$ spin Hall thin films on GaAs (111)A substrates”, Appl. Phys. Lett. 110 (2017) 062401-1-5.

[28] P. Sandstrom, E. B. Svedberg, J. Birch, J-E. Sundgren, “Structure and surface morphology of epitaxial Ni films grown on MgO (1 1 1) substrates: growth of high quality single domain films”, Journal of Crystal Growth 197 (1999) 849-857.

[29] Y. Fu, H. Lei, X. Wang, D. Yan, L. Cao, G. Yao, C. Shen, L. Peng, Yan Zhao, Y. Wang, W. Wu, “Fabrication of two domain Cu_2O (0 1 1) films on MgO (0 0 1) by pulsed laser deposition”, Applied Surface Science 273 (2013) 19– 23.

[30] R. Kuhl, W. Kraak, H. Haefner, and R. Herrmann, “The semimetal- semiconductor transition in bismuth- antimony alloys”, Phys. Stat. Sol. (b) 77 (1976) K109-111.

[31] E. S. Walker, S. Muschinske, C. J. Brennan, S. R. Na, T. Trivedi, S. D. March, Y. Sun, T. Yang, A. Yau, D. Jung, A. F. Briggs, E. M. Krivoy, M. L. Lee, “Composition-dependent structural transition in epitaxial Bi1−*x*Sb*x* thin films on Si(111)”, Phys. Rev. Mater. 3 (2019) 064201-1-8.

Kenneth M. Liechti,2 Edward T. Yu,1 Deji Akinwande,1 and Seth R. Bank1,*

[32] F. Y. Yang, Kai Liu, Kimin Hong, D. H. Reich, P. C. Searson, C. L. Chien, Y. Leprince-Wang, Kui Yu-Zhang, and Ke Han, “Shubnikov–de Haas oscillations in electrodeposited single-crystal bismuth films”, Phys Rev. B 10 (2000) 6631-6636.

Figure captions

Fig. 1: (a) Out-of-plane (2θ-θ) XRD patterns for BiSb films (x = ~0.1) formed on BaF_2 (111) substrates by a conventional procedure (one-step growth) and two-step growth. The upper or lower part of the XRD patterns correspond to those of BiSb films grown by one-step (1-step) or two-step (2-step) growth, respectively. (b) Intensity of the (003) XRD peak as a function of the growth temperature at the initial stage (T_{ini}). Solid circles and open triangles indicate c-axis oriented, single crystalline and polycrystalline BiSb films, respectively.

Fig. 2: SEM images of the BiSb films on BaF_2 (111) substrates formed by 2-step growth with the growth temperature at the initial stage (T_{ini}) of (a) 100°C, (b) 150°C and (c) 200°C.

Fig. 3: (a) Out-of-plane (2θ-θ) XRD patterns around the (003) peak for BiSb films with various Sb composition (x = 0.04–0.44) on BaF_2 (111) substrates. The composition x of each BiSb films was determined by EDX. (b) Dependence of the *c*-axis lattice constants of the BiSb films on the x (Sb composition). The dotted line shows the ideal *c* values estimated using Vegard's law.

Fig. 4: (a) In-plane XRD results (ϕ-scan) for BiSb (012) and BaF_2 (-111) for the BiSb films (x= ~0.1) formed on BaF_2 (111) substrates. (b) Reciprocal space mapping (RSM) for the BiSb films formed on BaF_2 substrates; the image shows around BiSb (2-19) and BaF_2 (135).

Fig. 5: (a) Out-of-plane (2θ-θ) XRD pattern for BiSb film (x = ~0.1) formed on a GaAs (111) substrate by two-step growth. (b) In-plane XRD results (ϕ-scan) for BiSb (012) and GaAs (-111) for BiSb film formed on a GaAs substrate.

Fig. 6: Temperature dependence of the (a) resistivity, and (b) electron concentration and mobility for $Bi_{0.96}Sb_{0.04}$, $Bi_{0.90}Sb_{0.10}$ and $Bi_{0.84}Sb_{0.16}$ films on BaF_2 (111) substrates.

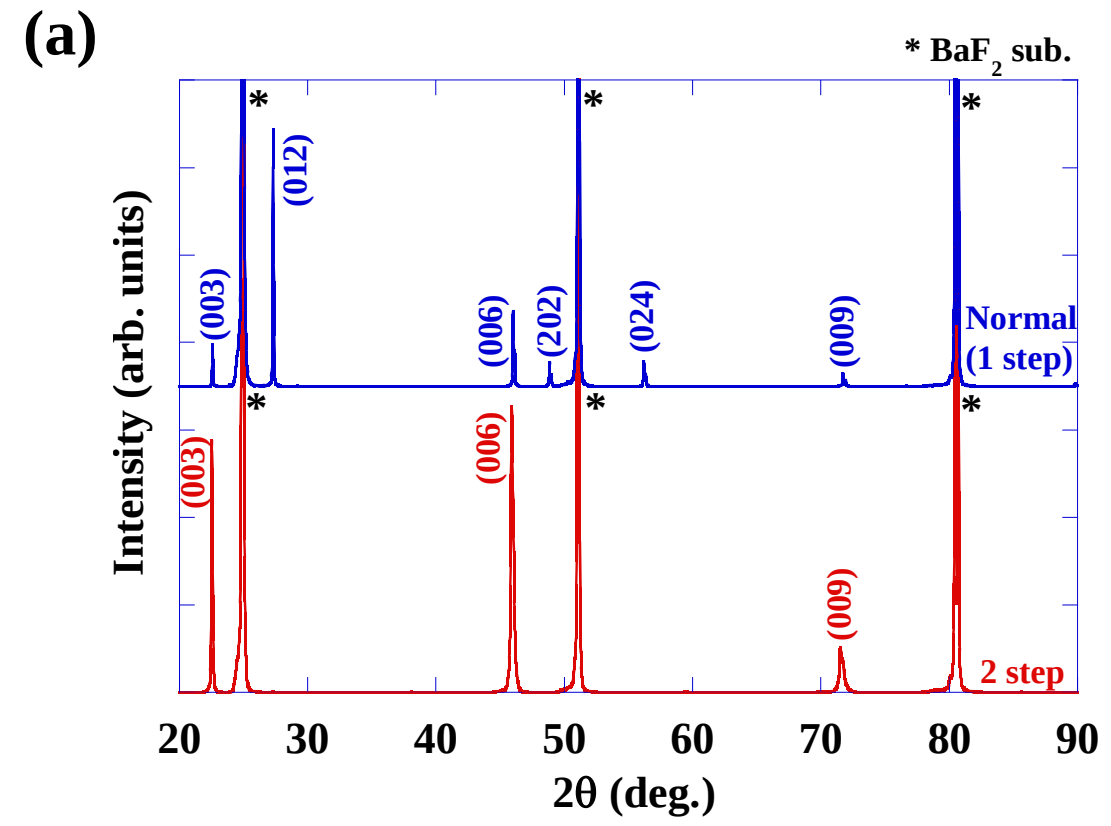
(a)
* BaF2 sub.
Intensity (arb. units)
(003)
(012)
(006)
(202)
(024)
(009)
Normal
(1 step)
(003)
(006)
(009)
2 step
20
30
40
50
60
70
80
90
2θ (deg.)

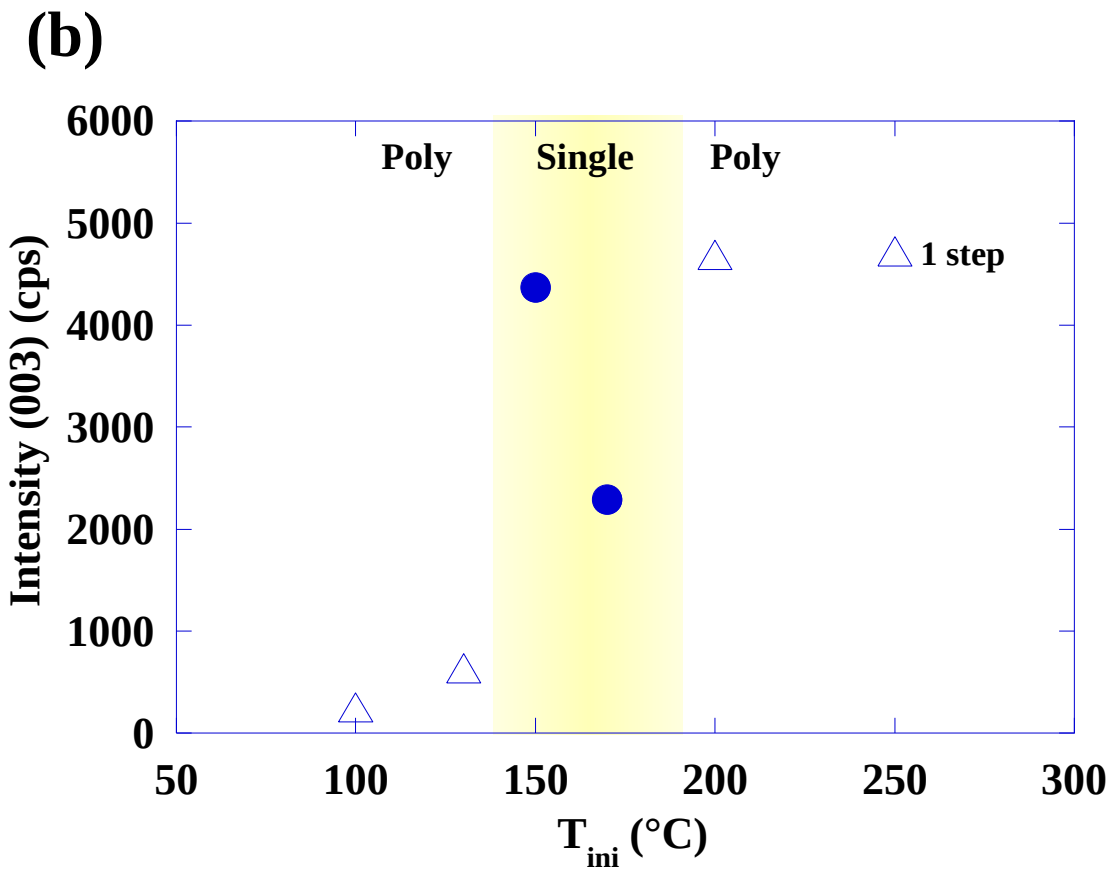
(b)
Poly
Single
Poly
1 step
Intensity (003) (cps)
6000
5000
4000
3000
2000
1000
0
50
100
150
200
250
300
T ini (°C)

Fig. 1

(a)

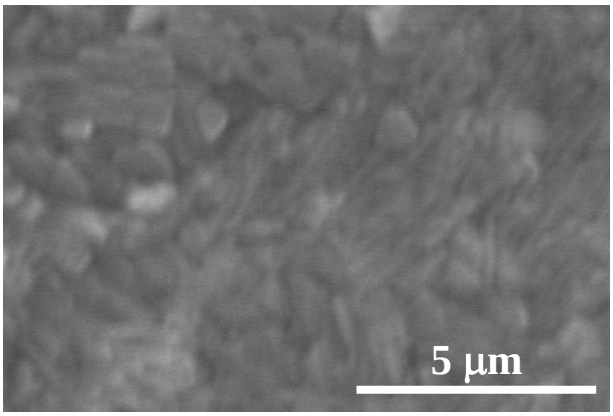

(b)

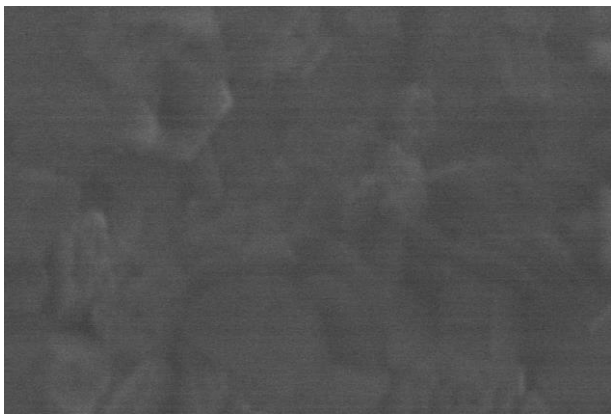

(c)

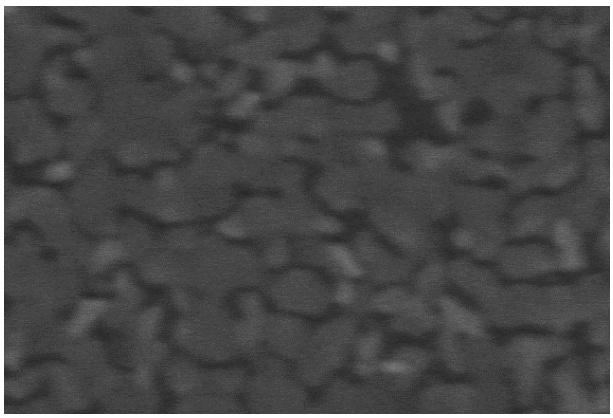

Fig. 2

(a)

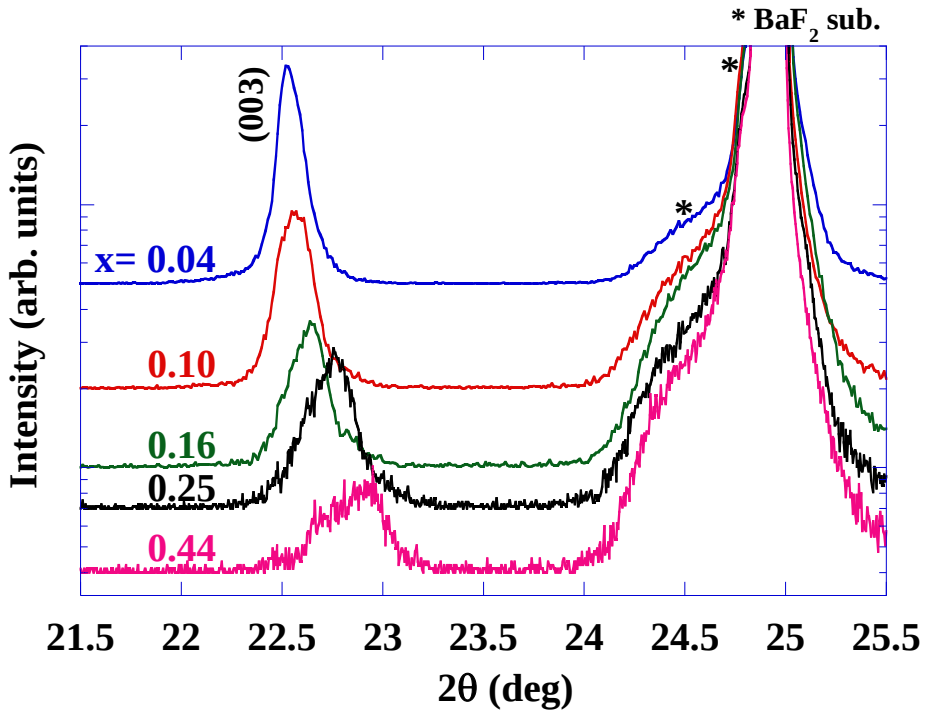
* BaF2 sub.
(003)
*
*
x= 0.04
0.10
0.16
0.25
0.44
Intensity (arb. units)
21.5
22
22.5
23
23.5
24
24.5
25
25.5
2θ (deg)

(b)

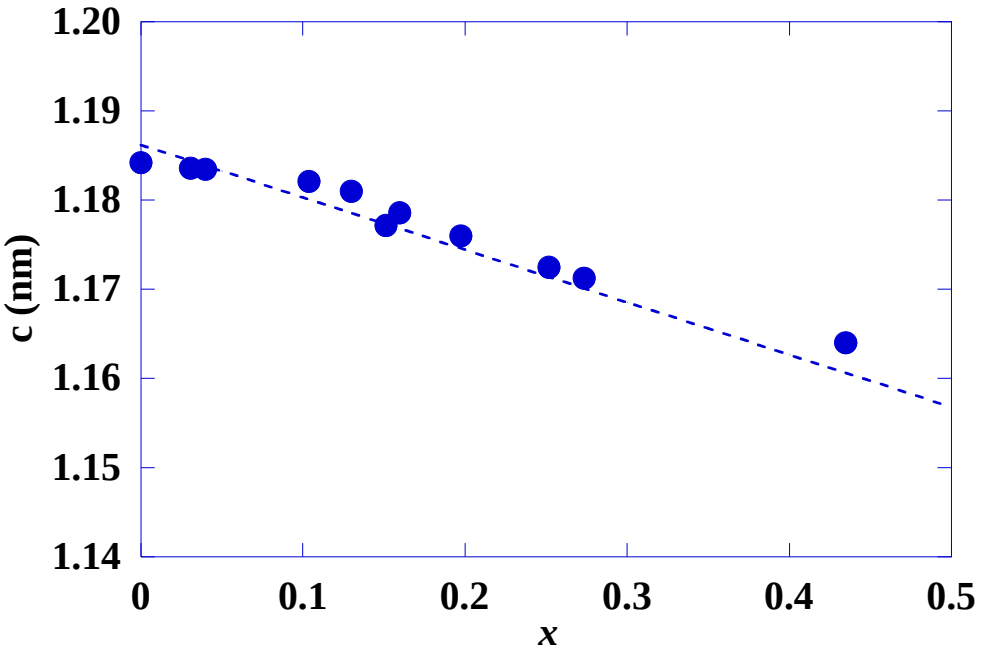
1.20
1.19
1.18
1.17
1.16
1.15
1.14
c (nm)
0
0.1
0.2
0.3
0.4
0.5
x

Fig. 3

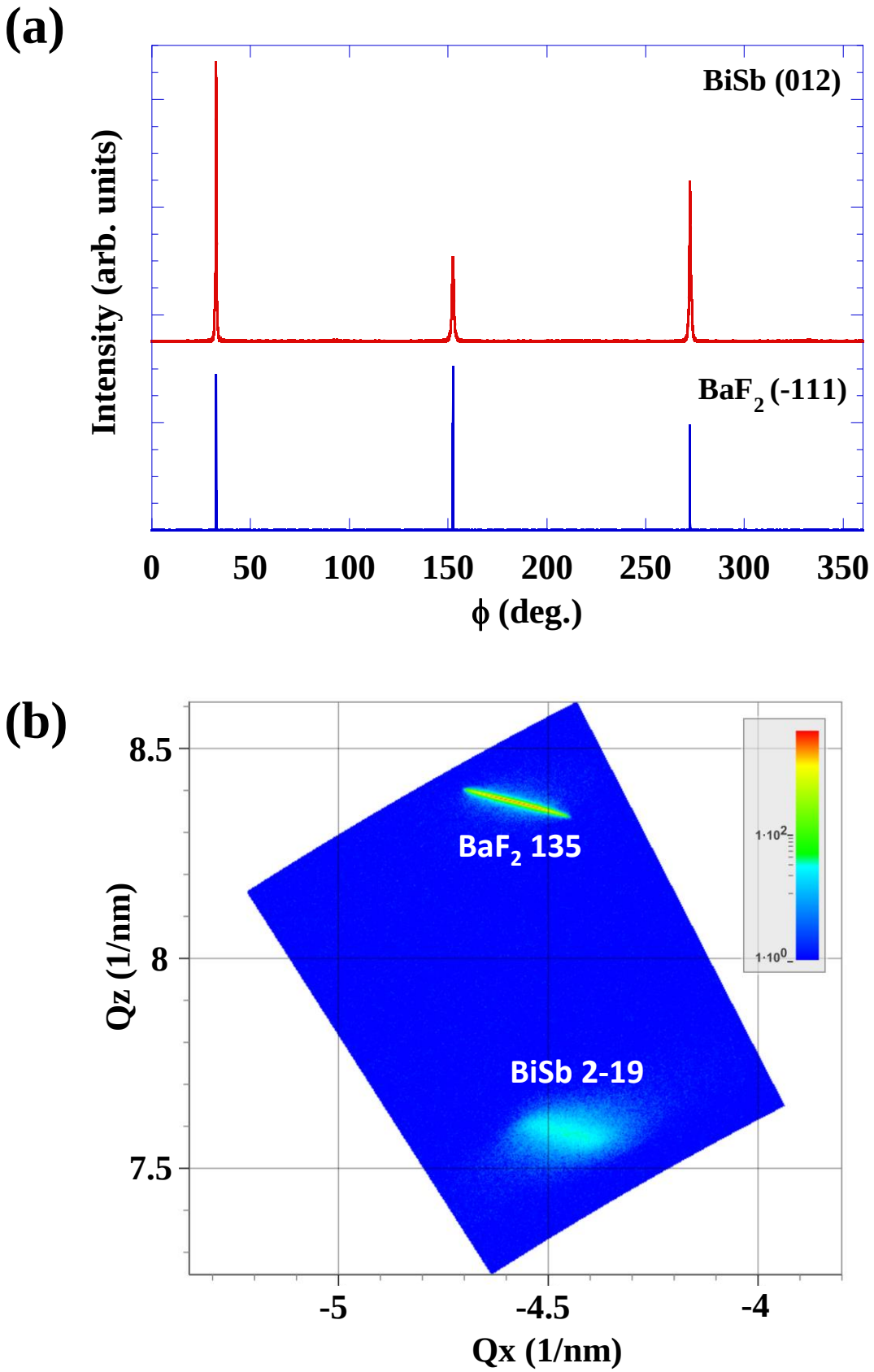
(a)
BiSb (012)
BaF2 (-111)
Intensity (arb. units)
0
50
100
150
200
250
300
350
ϕ (deg.)
(b)
8.5
8
7.5
Qz (1/nm)
BaF2 135
BiSb 2-19
1·10^2
1·10^0
-5
-4.5
-4
Qx (1/nm)

Fig. 4

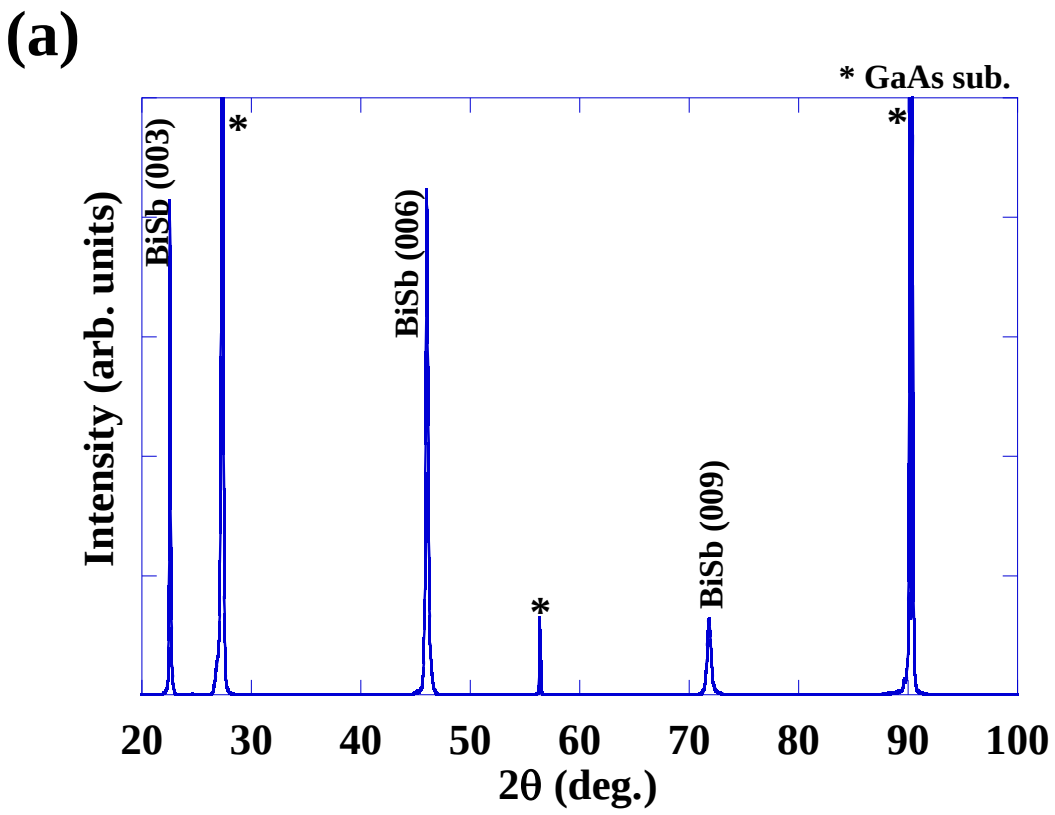
(a)
* GaAs sub.
BiSb (003)
BiSb (006)
BiSb (009)
*
Intensity (arb. units)
20
30
40
50
60
70
80
90
100
2θ (deg.)

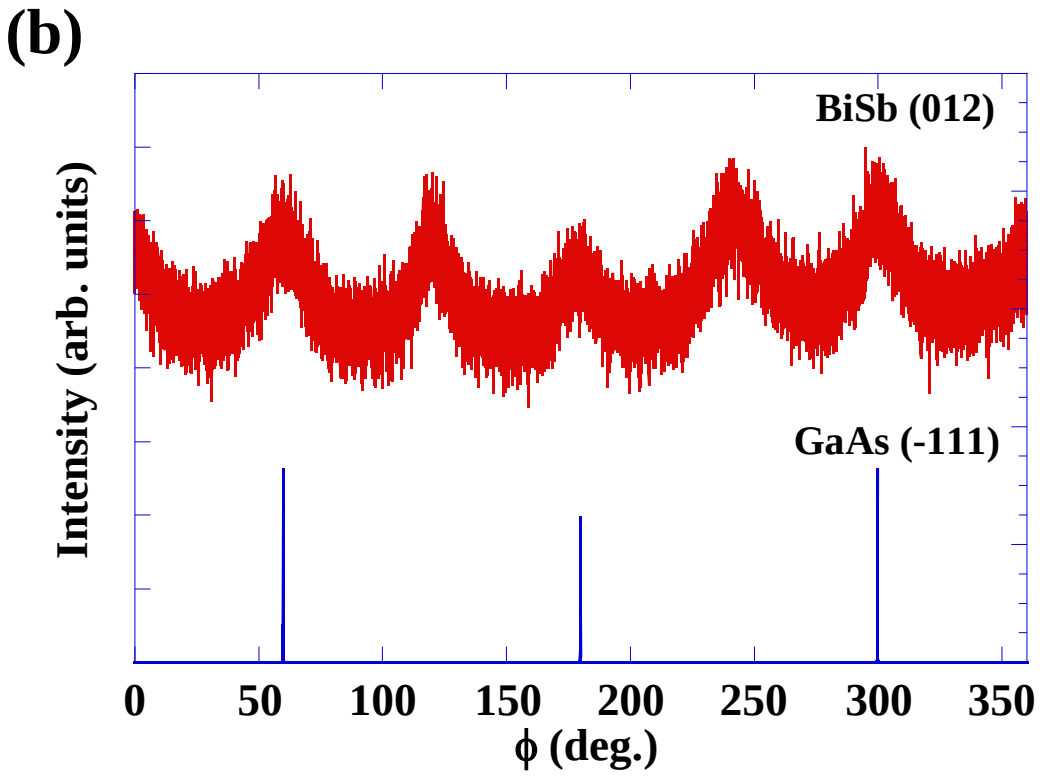
(b)
BiSb (012)
GaAs (-111)
Intensity (arb. units)
0
50
100
150
200
250
300
350
ϕ (deg.)

Fig. 5

(a)

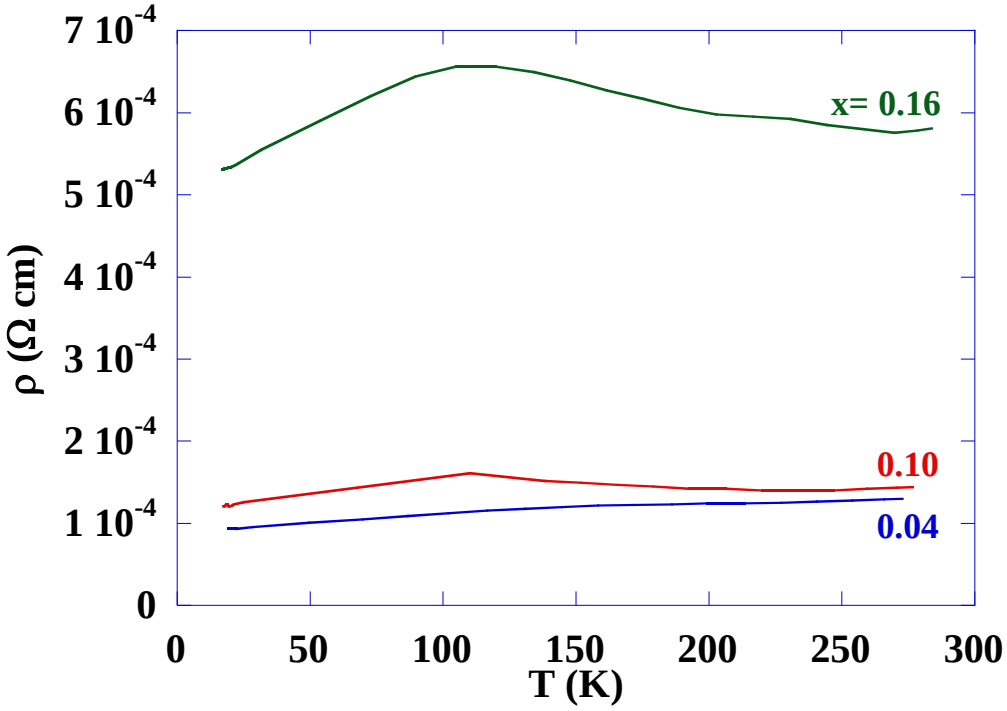
7 10-4
6 10-4
5 10-4
4 10-4
3 10-4
2 10-4
1 10-4
0
ρ (Ω cm)
x= 0.16
0.10
0.04
0
50
100
150
200
250
300
T (K)

(b)

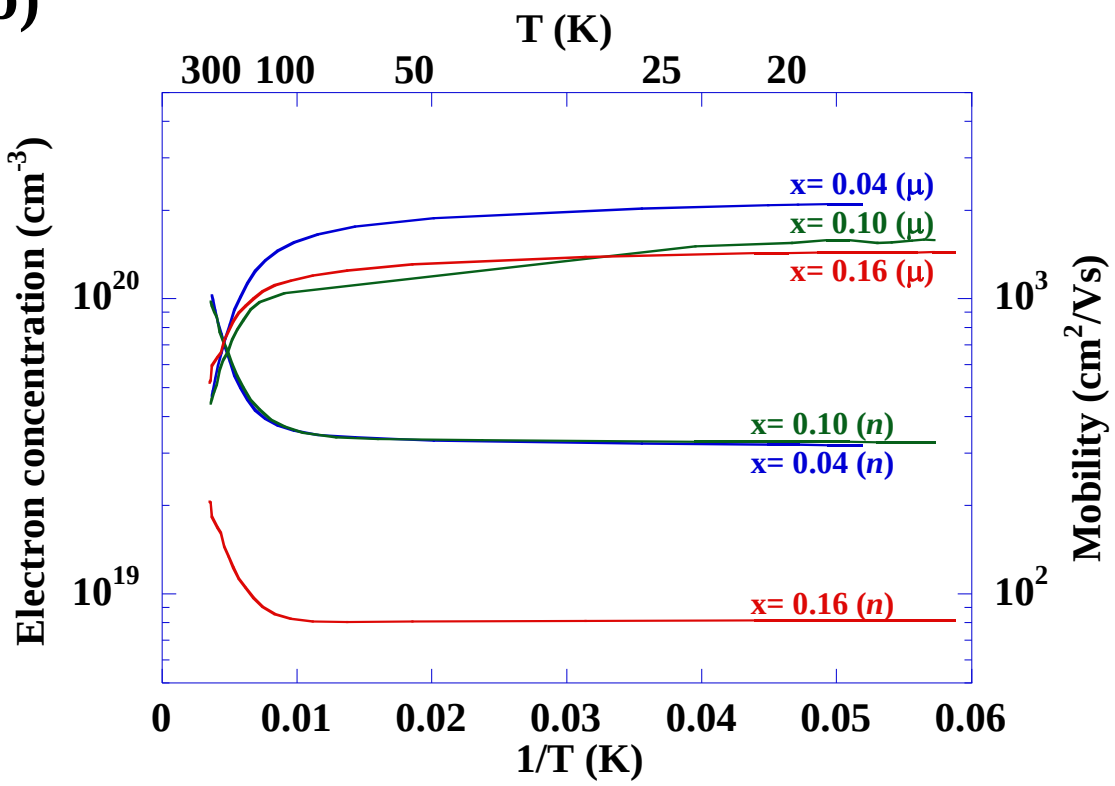
T (K)
300 100 50 25 20
Electron concentration (cm-3)
10^20
10^19
x= 0.04 (μ)
x= 0.10 (μ)
x= 0.16 (μ)
x= 0.10 (n)
x= 0.04 (n)
x= 0.16 (n)
10^3
10^2
Mobility (cm2/Vs)
0
0.01
0.02
0.03
0.04
0.05
0.06
1/T (K)

Fig. 6